Available online at www.sciencedirect.com
SCIENCE DIRECT
Thermochimica Acta 443 (2006) 147–158
thermochimica acta
www.elsevier.com/locate/tca

Effect of sample size on isothermal crystallization measurements performed in a differential scanning calorimeter: A method to determine avrami parameters without sample thickness effects

M.J. Hargis, B.P. Grady *

The University of Oklahoma, School of Chemical, Biological, and Materials Science, 100 East Boyd, EC Room T-223, Norman, OK 73019, United States

Received 19 October 2005; received in revised form 27 December 2005; accepted 28 December 2005
Available online 20 February 2006

Abstract

Isothermal crystallization studies of low-density polyethylene (LDPE) and high-density polyethylene (HDPE) using differential scanning calorimetry (DSC) were performed using different sample thicknesses to determine the effect of non-ideal heat-transfer. Polyethylene was chosen because of its importance, its extensive coverage in the literature, and its fast crystallization kinetics. Thermal gradients were found to significantly affect the measured crystallization exotherm; slower crystallization rates were observed for thicker samples measured at lower temperatures (greater supercoolings). Differences between different sample thicknesses disappeared at higher temperatures, consistent with finite heat-transfer rates being responsible for the effect. A power-compensation and a heat-flux DSC were used; these experiments also enabled the determination that the performance of the latter was acceptable for this study. Finally, thickness-independent Avrami parameters have been calculated.

Keywords: Isothermal crystallization; Differential scanning calorimetry; Polymers; Avrami equation

1. Introduction

Most processes involving a polymer melt include a cooling step where the melt becomes a solid. During the cooling step, semi-crystalline polymers develop crystalline regions; in the case of non-oriented polymer chains, the crystalline regions organize into spherulitic superstructures. The characteristics of the crystalline regions strongly affect the mechanical, optical, and other properties of the finished piece. Understanding the kinetics of the crystallization process is of utmost importance in the polymer processing industry.

Polymer crystallization kinetic research is often performed with differential scanning calorimetry (DSC) [1,2]. Compared to the rather large amount of attention paid to this same effect in scanning [3,4] and modulating [5–10] experiments, the amount of attention given to the analysis of sample heat-transfer effects in isothermal crystallization experiments in a DSC is rather small [11]. As with other types of experiments, the finite time for heat to flow through the DSC as well as undesirable heat paths may cause artifacts that are specific to the DSC design and performance. Further, some portion of the polymer sample may be significantly above the specified isothermal crystallization temperature because of low polymer thermal conductivity. Both of these issues are explored in this study.

Previous studies have modeled the effect of sample thermal conductivity on isothermal crystallization. In one pioneering work, it was realized that the heat released by a polymer melt upon crystallization could affect the kinetics of the crystallization [12]. A later study by the same author found that the internal temperature increase of a crystallizing polymer sample is significant and could distort isothermal crystallization rates [13]. However, both modeling studies used samples with thicknesses from 2 to 5 mm, much larger than thicknesses in typical DSC samples. Secondly, the study used a model with a crystallizing polymer sample of infinite width bound by two parallel plates held at a constant temperature. While this heat-transfer model is similar to the experimental setup in a typical DSC experiment, enough differences exist so that the degree to which the heat-transfer is effected in a DSC cannot be determined based on these studies alone.

* Corresponding author. Tel.: +1 405 325 4369; fax: +1 405 325 5813.
E-mail address: bpgrady@ou.edu (B.P. Grady).

0040-6031/$ – see front matter © 2006 Elsevier B.V. All rights reserved.
doi:10.1016/j.tca.2005.12.027

The only detailed experimental study that we are aware of concerning heat-transfer effects in isothermal crystallization experiments performed in a DSC indicated that medium density polyethylene and poly(oxymethylene) crystallize more slowly as the thickness is increased [11]. In our opinion, the Avrami kinetic parameters are not appropriately defined in this paper because the time where crystallization begins was not defined properly; this observation is apparent in the non-linearity of the data in Fig. 5 of ref. [9]. Further, one goal of our study, not explored in this previous study, was to determine a method to quantitatively describe changes in the rate of crystallization as a function of the sample size in a DSC and hence determine thickness-independent Avrami parameters.

The Avrami equation is used to describe the crystallization rate and assumes that constant, random nucleation occurs within the melt material and that spherulite growth is isotropic and constant [14,15]. Neither of these assumptions is absolutely correct since the sample has finite size; however, the success of applying this equation to DSC experiments speaks to the general correctness of the assumptions. Also, the Avrami equation assumes that the composition and structure of the melt remains constant during the crystallization process [16], which to a first approximation is true. The Avrami equation has the form:

$$\varphi_c = 1 - \exp(-k(t - \tau_0)^n) \quad (1)$$

where φ_c is the relative crystallinity (defined to be 1 when crystallization stops at a given isothermal temperature), k the Avrami isothermal crystallization rate constant, τ_0 the time at which isothermal crystallization begins, and n is the Avrami index. In Eq. (1), zero time is defined in some manner as to be the same independent of sample characteristics, i.e. the time where cooling begins. Many times τ_0 is not explicitly shown; in this situation zero time should be defined as when crystallization begins [17]. In either case, some rational way must be used to determine the time where crystallization begins. The time where crystallinity begins depends on DSC performance, temperature and sample thickness. Proper determination of the time where crystallinity begins is a critical issue, and will be discussed further in Section 2. In theory, the Avrami index should describe the geometry of crystallization growth and varies between 1 and 4. In practice, the Avrami index is a fitted parameter and, over the reasonably small temperature range investigated in these studies, should be independent of temperature. The isothermal crystallization rate constant "k" is strongly temperature-dependent. Theoretically, the parameter k encompasses all thermal effects, and trends in k (or $k^{1/n}$) should give excellent insight into changes in the crystallization rate between samples due to sample thermal conductivity. Using fitted Avrami parameters from isothermal crystallization experiments measured with samples of different thicknesses, k (or a function of k) can be extrapolate to zero thickness. A sample of zero thickness would have no internal temperature gradients, and the determined Avrami parameters would describe the true crystallization kinetics. The appropriate functional form to use in the extrapolation is also addressed in this paper.

2. Experimental

Low-density polyethylene (LDPE) and high-density polyethylene (HDPE) samples with different characteristics were investigated to explore the robustness of the procedures. Two LDPE samples were purchased from Aldrich; the melt-flow indexes (MFI) of these samples were 1.5 and 25. The third LDPE was graciously supplied by PFS Thermoplastics, now Innotek World Resins LLC, and had a melt index of 30. Three HDPE samples were graciously supplied by Exxon-Mobil Chemical; the MFIs were determined to be 4.90, 0.47, and 0.05 by ASTM method D 1238-04, procedure A. Hereafter, each sample will be referred to as either "LDPE" or "HDPE" followed by its melt-flow index.

Each polyethylene was compression molded into samples with varying thicknesses. The thickness variation of each sample was less than 0.01 mm. Very thin samples (thicknesses of the order of 0.05 mm) yielded inconsistent data presumably because of poor-sample pan contact and hence the results from these samples were not used. Aluminum pans with 0.63 mm (0.25 in.) diameters were used; the lids were pressed so that the top and bottom of the samples made contact with the aluminum. These samples were trimmed to fit the bottom of normal aluminum DSC pans. However, trimming the samples to fit perfectly inside the pans was not possible and hence samples are described by their mass rather than their thickness. In other words, changes in the sample thickness occurred due to spreading when the sample was melted. The change was not quantified; however, sample thickness should scale linearly with sample mass.

A TA Instruments Q1000 differential scanning calorimeter with liquid nitrogen cooling was used for this study, and was routinely calibrated with four different standards (cyclopentane, biphenyl, indium, and tin) at a 10 °C/min heating rate. The Q1000 software comes equipped with Advanced Tzero™, which theoretically eliminates the effect of thermal contact resistance between the instrument and the pan, as well as compensating for heat flow between the sample and the reference. Further, the instrument is designed to minimize heat-transfer resistance between the sample and the heat sink. Unlike most heat-flux DSCs, this instrument is deemed capable by the manufacturer for performing isothermal crystallization experiments even with fast crystallizing samples [18]. As recommended by the manufacturer, the PID controller parameters were tuned in order to minimize the time required to reach the specified temperature during a very fast cool. We found the best parameters for this temperature range were $P = 40$, $I = 0$, and $D = 5.0$.

Each sample was heated to 170 °C, which is above the equilibrium melting temperature for polyethylene [19], for a minimum of 5 min to ensure that the sample was completely melted. The sample was cooled in two steps at 75 °C/min, and the intermediate temperature was chosen so that the same temperature change was used for each cooling step. A controlled cool rather than a ballistic cool was used because the temperature profile was more consistent with a controlled cool. 75 °C/min was essentially the maximum constant cooling rate possible in this temperature range. Two steps were used so as to enable the separation of the exotherm due to cooling from that of crystallization. A 2-min

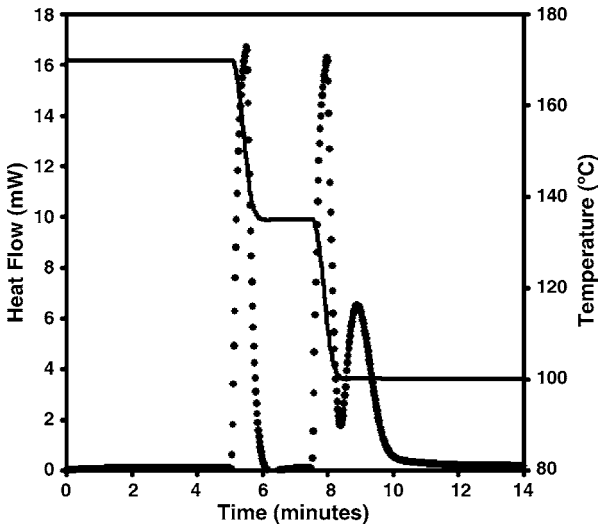

Fig. 1. Sample enthalpy and temperature vs. time for an isothermal crystallization experiment (line represents sample temperature, dots represent heat flow).

pause was necessary between cooling steps as determined by the enthalpy profile of the first step (see Fig. 1). After the second step, the sample was allowed to remain at the specified isothermal crystallization temperature as long as a crystallization exotherm was observed. This particular DSC has the characteristic that the user-specified temperature is not the actual temperature that the machine reaches; there is typically an approximate 0.5 °C offset, with the sample being at the higher temperature. In fact, the actual temperature reached was not exactly the same for all samples; the average standard deviation from the reported temperature for all samples is less than 0.04 °C. In the most extreme cases, the sample temperatures were within ±0.1 °C of the reported average. Actual average sample temperatures are reported in this paper. A quench cool followed by a ramp reheat at 10 °C/min was done to determine the properties of the melting transition. The crystallization enthalpy assumed for pure crystalline linear polyethylene was 282 J/g [20].

The subtraction required to isolate the exotherm due to crystallization from that due to cooling was performed by fitting the first cooling peak signal to the portion of the second cooling peak that was not convoluted with the crystallization exotherm. Of course, at higher crystallization temperatures there was no significant overlap. Two fitted parameters were necessary: a multiplicative term designed to take into account changes in the specific heat of the sample at different temperatures, and a constant term to taking into account baseline changes. This procedure appeared to be extremely accurate. After the fitting was performed, the modified first cooling peak was subtracted from the second cooling peak/isothermal crystallization peak. The resulting isothermal crystallization peak was numerically integrated to determine the relative crystallinity. This same procedure was used for data collected from both the heat-flux DSC and the power-compensation DSC.

A limited number of samples were measured on a power-compensation Diamond DSC manufactured by the Perkin-Elmer. Exactly the same samples (pans and polymer) were measured. Indium and zinc were used to calibrate the temperature; the former was used for enthalpy calibration. The samples and run parameters were supposed to have been exactly the same so that results could be directly compared between DSCs. However, there was a constant 1.5 °C temperature difference, as measured by the crystallization kinetics, between the two instruments with the power-compensation DSC at the higher temperature. It is well-known that temperature calibration upon heating is different than that upon cooling [21,22], and the systematic 1.5 °C difference is almost certainly related to differences in the heating/cooling calibration relationship between the two types of instruments. Comparisons described in the text take into account this difference, i.e. the shift in temperature has been applied to the power-compensation data.

The Avrami equation requires the assignment of when crystallization begins. We assumed time equals zero to be the time where the second cooling step began for both halftime determinations and Avrami kinetic analysis. The zero time is in fact arbitrary; the key is to accurately and consistently determine the value of τ_0. A consistent, but inaccurate, method to assign τ_0 is the time where the temperature reaches some arbitrary value with respect to the isothermal crystallization temperature. This approach is the one described in the appropriate ASTM standard [23]. Specifically, τ_0 is defined by the ASTM procedure as when the testing temperature reaches within 1 K of the specified temperature. Many problems exist with this definition, including the irrelevance of the actual cooling rate, the irrelevance of sample thickness, and the fact that, at low undercoolings (high temperatures), crystallization may not begin until well after that temperature is reached.

In order to determine τ_0 accurately and consistently, the Avrami equation was rearranged to the following linear form to determine τ_0:

$$\ln\left(\ln\left(\frac{1}{1-\varphi_c}\right)\right) = n\ \ln(t-\tau_0) + \ln(k) \tag{2}$$

The left hand side of the above equation was plotted against $\ln(t-\tau_0)$, and τ_0 was varied so that the range of relative crystallinities that was linear using this format was maximized. This approach resulted in the appropriate behavior of the Avrami equation, with deviation from linearity occurring only at high crystallization fractions. Further, this procedure resulted in the appropriate τ_0 behavior at low temperatures. If τ_0 represents the time where crystallization begins, then crystallization should start at approximately the same time if the crystallization temperature is low enough since only instrument performance will determine this time; data in Tables 1 and 2 show this behavior. Linear least squares fitting was used to determine the Avrami parameters over the relative crystallinity range between 5 and 75%. Model-independent crystallization halftimes were also identified and reported.

3. Results and discussion

3.1. Crystallization halftimes

Fig. 2 shows relative crystallinity versus crystallization time for different sample thicknesses of HDPE 4.9, and indicates the

Table 1
Avrami constants for LDPE samples

LDPE 1.5 (mg)		97.0 °C	98.5 °C	100.1 °C	101.6 °C	103.1 °C	104.6 °C	106.0 °C
13.47	k	9.289	20.852	1.767	1.263	0.339	0.152	0.055
	n	1.809	2.311	1.514	1.534	1.266	1.464	1.295
	τ_0	0.77	0.82	0.92	1.05	1.28	4.30	4.86
5.33	k			1.307	0.197	0.076	0.031	
	n			1.800	1.587	1.372	1.398	
	τ_0			0.96	0.96	1.75	2.8	
3.50	k	11.609	10.958	3.279	0.410	0.098	0.039	0.024
	n	1.772	2.623	1.700	1.290	1.383	1.00	1.200
	τ_0	0.71	0.71	0.88	1.19	1.75	3.60	4.80
1.78	k	10.144	14.949	1.378	0.330	0.155	0.040	
	n	1.597	1.963	1.478	1.365	1.525	1.261	
	τ_0	0.65	0.73	0.97	1.15	1.74	3.30	
LDPE 25 (mg)		97.0 °C	98.6 °C	100.1 °C	101.6 °C	103.1 °C	104.6 °C	106.0 °C
14.82	k	9.741	8.0591	3.698	3.848	1.523		
	n	1.640	1.660	1.536	1.791	1.853		
	τ_0	0.73	0.77	0.83	0.96	1.10		
6.15	k		22.379	8.743	2.837	0.692	0.082	0.030
	n		2.010	1.732	2.554	1.739	1.466	1.738
	τ_0		0.75	0.85	0.78	1.13	2.15	2.40
2.44	k	76.971	46.703	27.286	4.628	0.791	0.103	0.020
	n	2.112	2.169	2.521	2.209	2.397	2.029	2.117
	τ_0	0.68	0.71	0.79	0.83	0.85	1.20	1.21
1.25	k	286.965	117.282	16.860	7.181	0.879	0.057	0.030
	n	2.807	2.705	2.261	2.573	1.759	2.848	1.890
	τ_0	0.64	0.68	0.74	0.76	1.05	0.71	1.70
LDPE 25: Power-compensation DSC (mg)			98.7 °C	100.2 °C	101.7 °C	103.1 °C	104.6 °C	106.1 °C
	6.15	k	16.876	6.295	1.913	0.369	0.047	0.012
		n	1.762	1.729	1.979	2.021	1.924	1.568
		τ_0	1.145	1.193	1.264	1.392	1.582	2.302
	1.25	k	29.184	13.938	3.552	0.110	0.112	0.024
		n	1.749	1.924	2.131	1.922	1.910	1.577
		τ_0	1.168	1.191	1.211	1.552	1.542	1.662
LDPE 30 (mg)		97.2 °C	98.5 °C	100.1 °C	101.5 °C	103.0 °C	104.5 °C	106.0 °C
17.16	k	3.648		1.298	0.348	0.106	0.062	0.013
	n	1.789		1.857	1.779	1.786	1.432	1.526
	τ_0	0.83		1.00	1.14	1.51	3.05	8.42
5.27	k	15.669	4.583	1.119	0.488	0.127	0.045	0.014
	n	2.030	1.962	1.721	1.752	1.764	1.630	1.545
	τ_0	0.74	0.81	0.85	0.99	1.35	2.45	4.55
3.17	k	17.310	8.005	1.870	0.576	0.119	0.028	0.005
	n	2.054	2.316	1.869	1.895	1.778	1.714	1.799
	τ_0	0.74	0.76	0.85	0.93	1.25	2.35	2.65
1.64	k	43.123	11.028	3.654	0.749	0.191	0.032	
	n	2.600	2.106	2.095	1.961	1.762	1.700	
	τ_0	0.68	0.78	0.84	0.99	1.77	2.48	

All tables were determined with the heat-flux DSC unless otherwise noted, and all determined values are listed with the following units: k, $(\text{min})^{-n}$; n, dimensionless; τ_0, min.

significance of sample size in isothermal crystallization experiments. Crystallization halftimes shown in Figs. 3–6 on both linear and logarithmic axes; logarithmic plots are presented for better data resolution at high halftimes, linear plots for better data resolution at low halftimes. The plots indicate that thicker samples crystallize more slowly at faster crystallization rates, and that the effect disappears at slower crystallization rates. This behavior is expected if thermal conductivity affects the crystal-

Table 2
Avrami constants for HDPE samples

HDPE 0.47 (mg)		118.5 °C	112.0 °C	121.4 °C	122.9 °C	124.4 °C	125.9 °C	127.4 °C
17.16	k	2.233	1.868	1.488	0.603	0.104	0.010	
	n	1.357	1.385	1.486	1.534	1.949	1.867	
	τ_0	0.63	0.70	0.83	1.07	1.78	7.12	
5.27	k	8.727	4.953	2.896	1.524	0.217	0.007	4.33×10^{-6}
	n	1.535	1.292	1.393	1.509	1.897	2.275	2.821
	τ_0	0.55	0.63	0.72	0.90	1.54	4.80	9.45
3.71	k	11.914	7.325	4.266	1.372	0.161	0.002	7.53×10^{-6}
	n	1.635	1.532	1.583	1.654	2.059	2.420	2.468
	τ_0	0.61	0.66	0.76	0.92	1.63	5.10	3.00
1.64	k	50.602	17.839	9.020	3.198	0.232	0.006	8.47×10^{-6}
	n	1.842	1.610	1.638	2.041	2.118	2.389	2.589
	τ_0	0.59	0.63	0.75	0.89	1.47	4.60	6.42

HDPE 0.47: Power-compensation DSC (mg)		120.0 °C	121.5 °C	124.0 °C	124.5 °C	126.0 °C
5.27	k	5.073	3.166	1.354	0.047	0.002
	n	1.235	1.444	1.720	2.183	2.084
	τ_0	0.873	0.927	1.107	2.397	10.607
1.64	k	7.299	7.620	2.065	0.153	0.001
	n	1.206	1.568	1.991	2.190	2.737
	τ_0	0.867	0.920	1.059	1.677	4.007

HDPE 0.05 (mg)		118.5 °C	112.0 °C	121.4 °C	122.9 °C	124.4 °C
16.25	k	1.645	1.039	0.171	0.025	2.95×10^{-5}
	n	1.417	1.532	1.906	1.899	2.671
	τ_0	0.77	0.92	1.15	4.20	14.50
7.99	k	3.182	1.893	0.216	0.035	2.41×10^{-4}
	n	1.586	1.479	1.673	1.907	2.415
	τ_0	0.66	0.80	0.87	2.75	6.60
2.80	k	2.864	1.970	0.204	0.035	1.75×10^{-4}
	n	1.472	1.528	1.728	1.907	2.496
	τ_0	0.67	0.80	0.84	2.73	6.00
2.01	k	10.297	3.061	0.365	0.014	3.00×10^{-4}
	n	1.745	1.685	2.034	2.180	2.270
	τ_0	0.69	0.82	1.03	2.60	5.80

HDPE 4.9 (mg)		118.5 °C	112.0 °C	121.4 °C	123.0 °C	124.5 °C	125.9 °C
16.77	k	2.301	1.408	0.465	0.026	0.002	
	n	1.598	1.794	2.173	2.665	2.601	
	τ_0	0.72	0.83	1.00	1.35	3.90	
7.92	k	4.707	3.082	0.516	0.016	0.002	4.30×10^{-4}
	n	1.690	1.908	2.349	3.252	2.879	1.893
	τ_0	0.65	0.75	0.75	0.50	2.20	4.00
3.86	k	18.837	1.179	1.179	0.024	9.63×10^{-4}	1.96×10^{-4}
	n	2.327	2.311	2.139	3.141	2.978	2.266
	τ_0	0.61	0.68	0.85	0.50	0.50	1.20
1.72	k	16.256	10.730	1.012	0.041	0.001	5.10×10^{-4}
	n	2.164	2.661	2.730	2.794	3.127	2.105
	τ_0	0.62	0.66	0.67	0.25	0.50	2.40

All tables were determined with the heat-flux DSC unless otherwise noted, and all determined values are listed with the following units: k, $(\text{min})^{-n}$; n, dimensionless; τ_0, min.

lization rate, since at higher temperatures the amount of heat released per unit time due to crystallization will be substantially less. The thickness-independent behavior at high temperatures (low undercoolings) also shows that thermal gradients in the thickness direction of the sample due to the cooling temperature profile can be ignored in these samples. Thermal gradients in the thickness direction due to cooling would also reduce the rate of crystallization in thicker samples, however with time con-

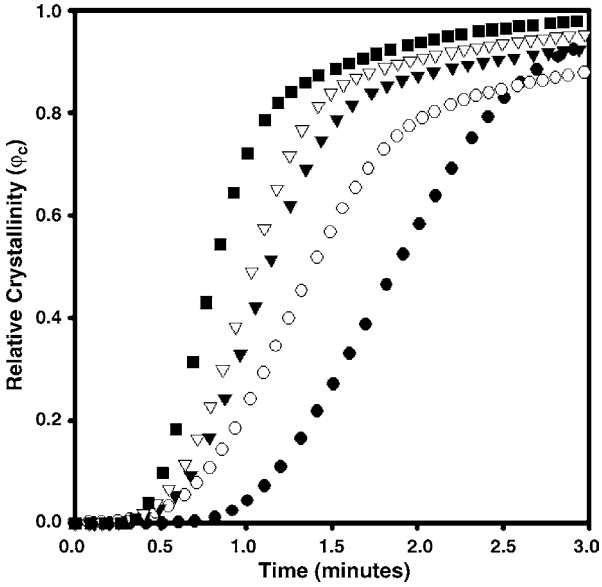

Fig. 2. Isothermal crystallization vs. time for different sample thicknesses of HDPE 4.9: 16.77 mg (●), 7.92 mg (◯), 3.86 mg (▼), 1.72 mg (▽), and 0.38 mg (■).

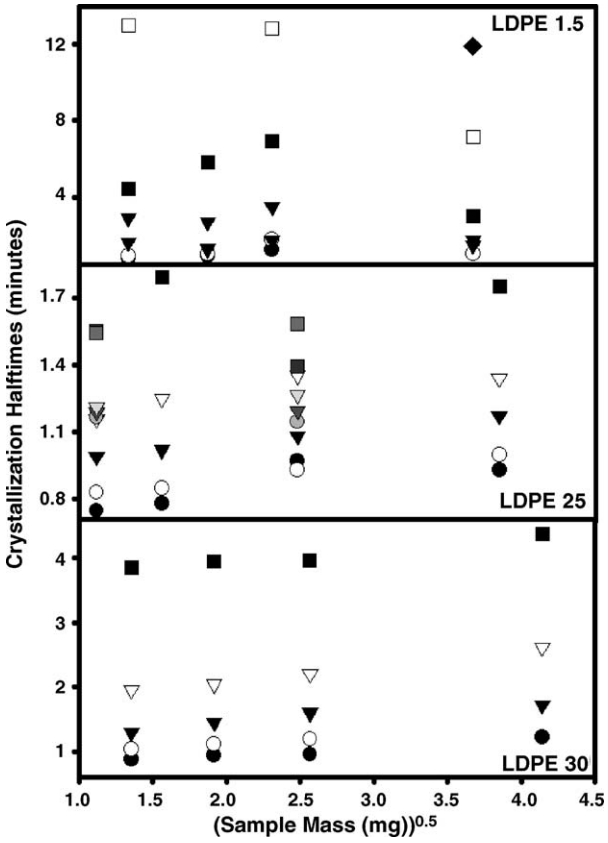

Fig. 3. Crystallization halftime vs. the square root of sample mass for all LDPE samples on a linear axis: 97.0 °C (●), 98.6 °C (◯), 100.1 °C (▼), 101.6 °C (▽), 103.1 °C, (■), 104.6 °C (□), and 106.1 °C (♦). Grey symbols indicate the sample was measured in the power-compensation DSC, with dark grey and light grey symbols representing their black and hollow heat-flux equivalents.

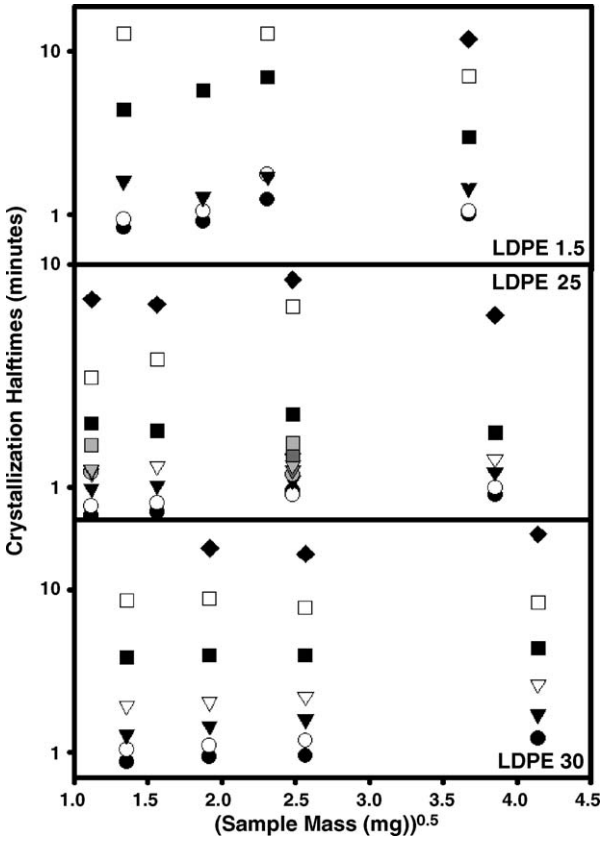

Fig. 4. Fig. 3 on a logarithmic axis for better data resolution.

stants on the order of seconds or less [24], this effect should be small.

Rather than heating due to the exothermic crystallization process, another possible explanation of the change in halftime with sample thickness is that the heat-flux DSC is not dissipating the generated heat rapidly enough; i.e. heat flow from the bottom of the pan to the heat sink limits the ability of the DSC to measure fast kinetics. One way to explore this possibility is to measure the same samples on a power-compensation DSC, where the rate of heat-transfer from the bottom of the pan to the heat sink is much faster. As seen in Figs. 3–6, the halftimes between the different DSCs are comparable, indicating that the heat-flux DSC is not significantly distorting the measurement. In fact, the halftimes of the power-compensation DSC were slightly longer, which we attribute to the fact that the PID parameters were not optimized for fast cooling steps in this instrument. In any case, the inherently slower heat-transfer ability in the heat-flux instrument is not measurably affecting the data, and the instrument is not the largest source of heat-transfer resistance.

3.2. Crystallization enthalpy

Figs. 7 and 8 are plots of the crystallization enthalpy versus isothermal crystallization temperature for each sample. The data scatter is quite large due to the sensitivity of the crystallization enthalpy to baseline determination; errors in cooling exotherm subtraction do not seem as significant. The crystallization exotherm decreases with increasing crystallization tem-

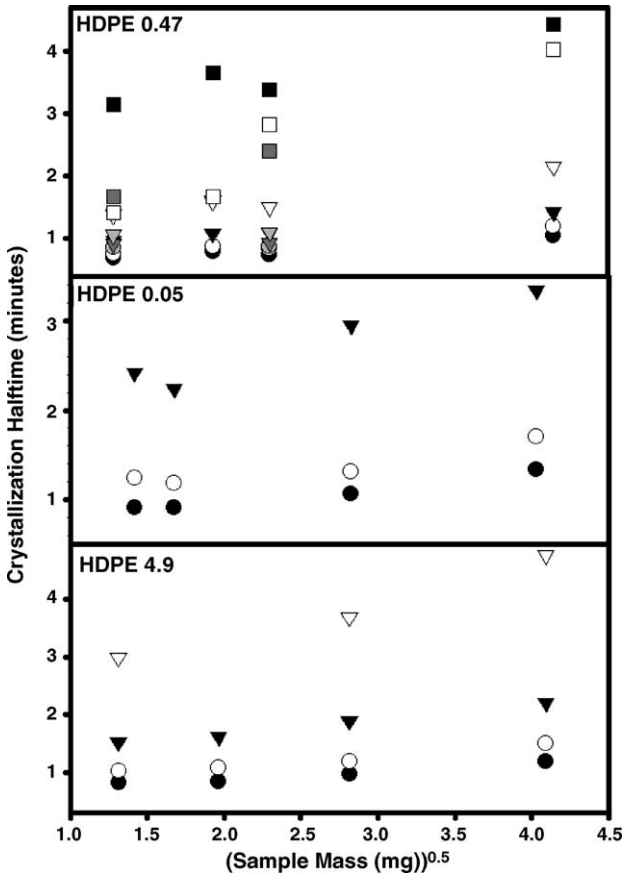

Fig. 5. Crystallization halftime vs. the square root of sample mass for all HDPE samples on a linear axis: 118.5 °C (●), 120.0 °C (◯), 121.4 °C (▼), 122.9 °C (▽), 124.4 °C, (■), 125.9 °C (□), and 127.4 °C (♦). Grey symbols indicate the sample was measured in the power compensation DSC, with dark grey and light grey symbols representing their black and hollow heat-flux equivalents.

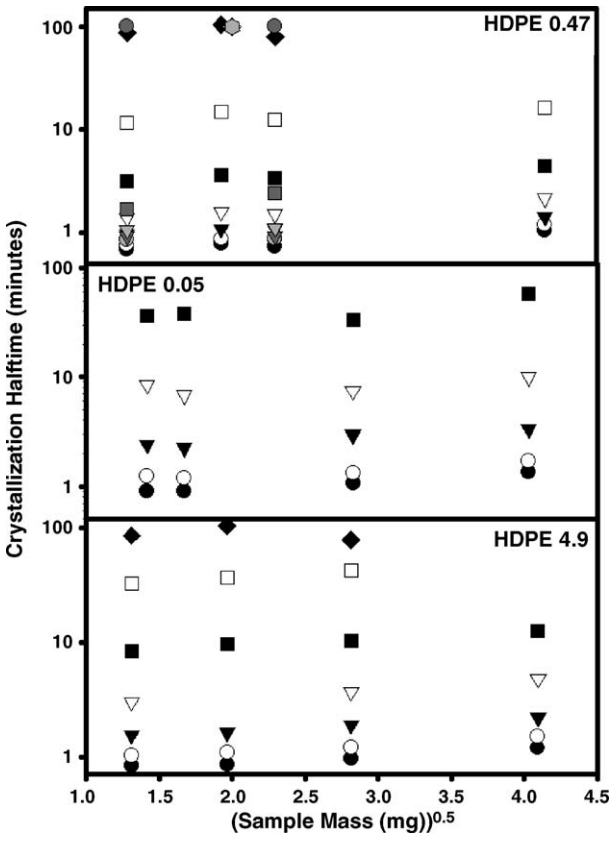

Fig. 6. Fig. 5 on a logarithmic axis for better data resolution.

perature indicating that higher overall fractional crystallinities are reached at lower crystallization temperatures. The enthalpy of crystallization measured during the cool after isothermal crystallization segment increased with increasing isothermal crystallization temperature, which also indicates that higher crystalline fractions during isothermal crystallization were reached at lower isothermal crystallization temperatures. Summing the enthalpies during the isothermal portion and the cool down portion did not consistently yield the measured enthalpy during the reheat, which we attributed to the difficulty in baseline determination at the beginning of the cool down portion of the cycle. The significant amount of data scatter prevented any conclusions to be made regarding the variation of enthalpy with sample size although there appears to be no effect. The energy required during the reheat was independent of isothermal crystallization temperature.

3.3. Avrami fits

As noted earlier, τ_0 was optimized by maximizing the range of the linear portion of the curve shown in Fig. 9. Increasing τ_0 from its optimal value caused premature downward curvature at high φ_c, while decreasing τ_0 from its optimal value caused upward curvature at low φ_c. In essence, the data is being forced to conform to a semi-empirical expression, which is a somewhat questionable procedure; however, all conclusions drawn in this section are supported by the observations made with model-independent crystallization halftimes. Even with this procedure to determine τ_0, high values of φ_c, i.e. values greater than about 75%, are not well-represented by the Avrami expression because of secondary crystallization. The values of τ_0 from the procedure described in conjunction with Eq. (2) accurately described the observed onset of crystallization as determined by inspection.

Very surprisingly, values of τ_0 were smaller at low crystallization temperatures when measured with the heat-flux DSC; as mentioned earlier the controller parameters were not optimized for the power-compensation DSC. The value of τ_0 increased with temperature and decreased with decreasing sample size, both were expected. At low temperatures, the difference between the τ_0 values for the two instruments was independent of temperature; however, this difference was not maintained as the temperature increased. We do not know the reason why the time difference was not maintained at higher temperatures. Also, fitted parameters from samples with higher melt-flow indices were more consistent reflecting perhaps that sample-pan contact is more reproducible for the materials with lower viscosities.

The Avrami parameters, along with values of τ_0 for each sample, are given in Tables 1 and 2. The Avrami exponent varies randomly as a function of temperature and sample thickness, as expected. The Avrami exponent varied from one to two for all

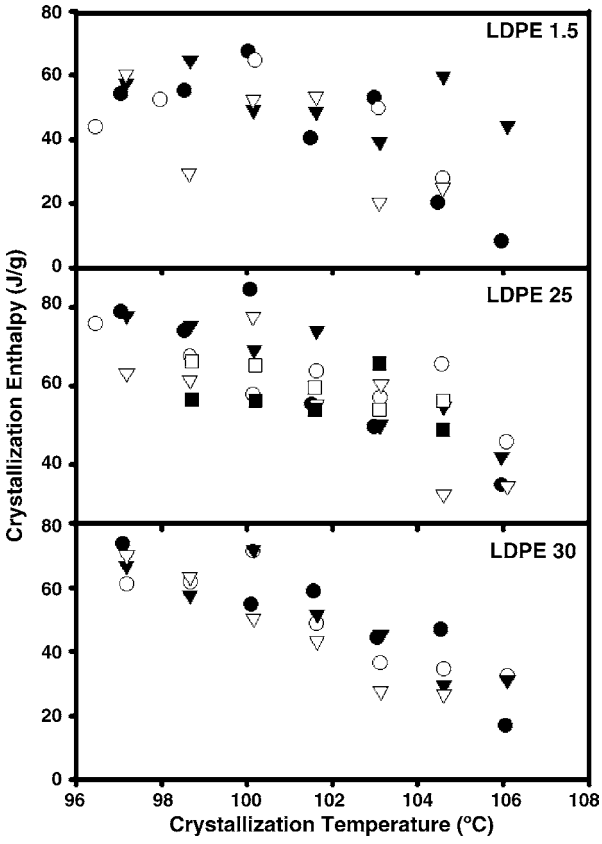

Fig. 7. Determined crystallization enthalpies for all LDPE samples for LDPE 1.5: 13.47 mg (●), 5.33 mg (◯), 3.50 mg (▼), and 1.78 mg (▽); for LDPE 25: 14.82 mg (●), 6.15 mg (◯), 2.44 mg (▼), 1.25 mg (▽), PE 1.25 mg (■) and PE 6.15 mg (□); for LDPE 30: 17.16 mg (●), 6.59 mg (◯), 3.68 mg (▼), and 1.84 mg (▽).

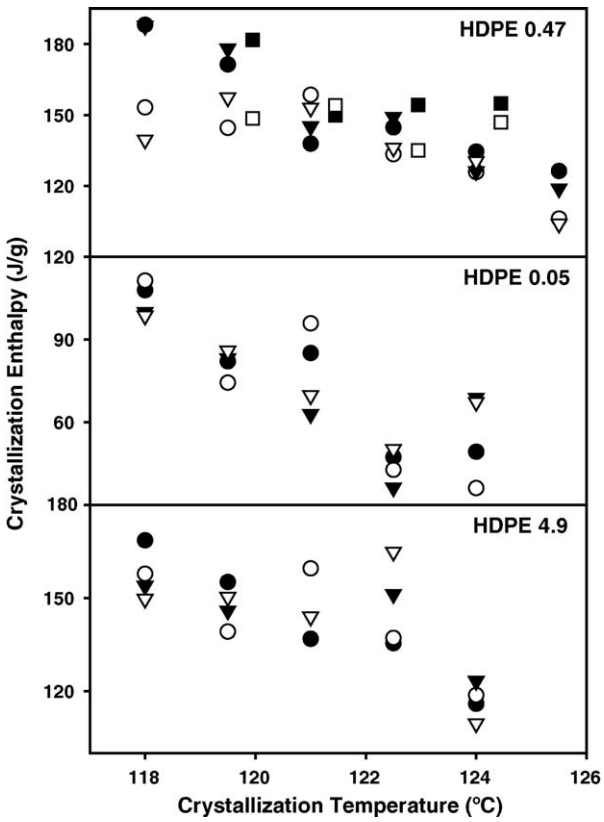

Fig. 8. Determined crystallization enthalpies for all HDPE samples for HDPE 0.47: 17.16 mg (●), 5.27 mg (◯), 3.71 mg (▼), 1.64 mg (▽), PE 1.64 mg (■), and PE 5.27 mg (□); for HDPE 0.05: 16.25 mg (●), 7.99 mg (◯), 2.80 mg (▼), and 2.01 mg (▽); for HDPE 4.9: 16.77 mg (●), 7.92 mg (◯), 3.86 mg (▼), and 1.72 mg (▽).

samples, except for HDPE 4.9 where the exponent generally varied between two and three.

With the most commonly used assumptions, specifically that spherulites grow as spheres and that no new spontaneous nucleation occurs after crystallization begins, k is proportional to the crystal growth rate G as follows [16]:

$$k = \frac{4\pi}{3}\left(\frac{\rho_c}{\rho_m}\right) G^n \tag{3}$$

This expression indicates that a plot of $k^{1/n}$ versus some function of the sample size should be examined for changes in the crystalline growth rate due to thermal gradients inherent in larger samples. From analytical expressions for any reasonable relevant geometry, the internal sample temperature should vary with the square of the thickness [25]. However, these solutions do not account for the fact that heat generation is inversely related to temperature. In other words, sample temperature is self-regulating since the exothermic heat release decreases as the temperature increases. An expression of G for polyethylene (μm/s) as a function of absolute temperature can be described as follows [26,27]:

$$G = G_0 \exp\left(\frac{-C}{T(\Delta T)}\right) \tag{4}$$

where G_0 and C are constants, T is the temperature in Kelvin, and ΔT is the supercooling in Kelvin.

A finite difference model was constructed in order to explore what empirically proper functional form should be used from

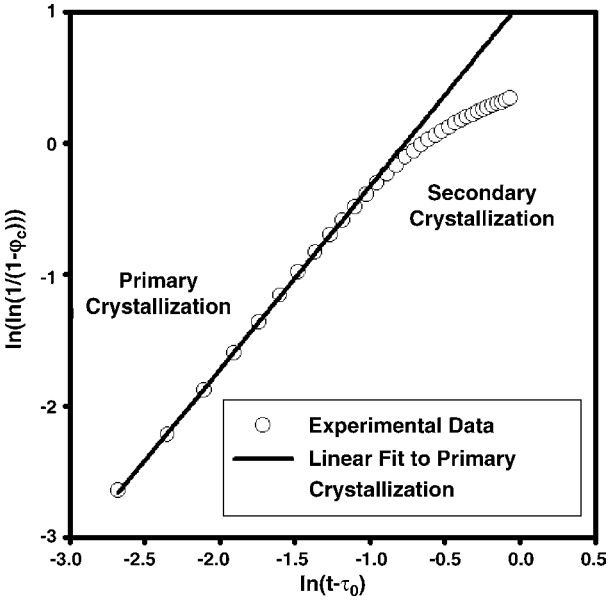

Fig. 9. Linearized Avrami fit showing distinct primary and secondary crystallization regions. Sample is HDPE 0.47 crystallized at 121.4 °C.

mass (or thickness) in order to best extrapolate $k^{1/n}$ to zero. A HDPE sample was divided into sections, and heat-transfer was determined using the temperature difference between the sections. The heat generated through crystallization was modeled using the average Avrami exponent n determined through our experiments, and the expression for the Avrami rate constant k in Eqs. (3) and (4). Parameters G_0 and C published elsewhere for HDPE based on optically measured growth rates in transcrystallinity experiments [33] were used; these parameters did an excellent job of reproducing our experimentally determined, thickness-independent $k^{1/n}$ values after conversion to the proper form. Heat-transfer between the sample and the DSC pan was assumed to be very fast, i.e. the temperatures of the layers touching the top and bottom of the sample pan, respectively, were assumed to be the specified isothermal crystallization temperature. Initially, the sample was also assumed to be at the specified isothermal crystallization temperature; admittedly this assumption is different from reality. For a given total thickness, the average temperature of the sample with time was constant and higher than the specified temperature because of the self-regulating heat release rate described earlier. This type of self-regulating isothermal behavior, for the same reasons, is seen in rapidly-cooled samples at higher supercoolings in a series of papers by Spruiell and co-workers and Wagner and Phillips [28–31]. Drastic changes in the average sample temperature were only noted at the start of crystallization and at the near-completion of the sample crystallization. The average sample temperature increased with increasing sample thickness. Five milligram samples were 0.5 °C above the specified DSC temperature, while 15 mg samples were 1.5 °C higher. The average sample crystallinity at a given time was determined by summing over the various slices, and the Avrami parameters were determined in the same manner detailed previously.

Although the agreement was not perfect, model results showed that $k^{1/n}$ should scale with the square of the sample thickness. As will be seen, this dependence was not found in the experimental data. More disturbing, n increased markedly with sample thickness, a trend not present in our experimental data. The model results did depend slightly on the number of slices used in the simulation; however, the increase in n did not depend on whether the thickness was varied by increasing the number of slices or the thickness of a slice. Given the qualitative mismatch between the model and the observed results, we were not able to gain any insight into the proper form to use for the extrapolation.

Logarithmic plots of $k^{1/n}$ versus the square root of the sample thickness are presented in Figs. 10 and 11 to show that the slope is non-zero and negative only at higher crystallization rates. Different values of x were used in a plot of $k^{1/n}$ versus $(\text{mass})^x$ in order to determine the best empirical form for a linear fit. As seen in Fig. 12, $\text{mass}^{1/2}$ was found to be the best functional form; the correlation coefficient was maximized as a function of x and, for most samples, the optimal value of x was between 0.4 and 0.6. This procedure enabled extrapolation of k to zero thickness, and this value should theoretically be the true Avrami kinetic rate constant since no heat-transfer effects should be present. The

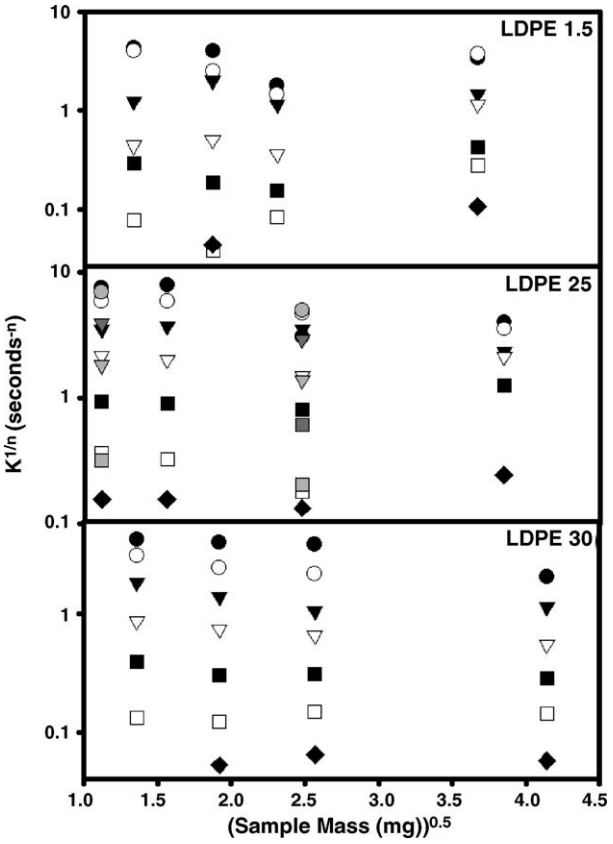

Fig. 10. Plot of $k^{1/n}$ vs. the square root of the sample mass for LDPE samples on a logarithmic scale: 97.0 °C (●), 98.6 °C (◯), 100.1 °C (▼), 101.6 °C (▽), 103.1 °C (■), 104.6 °C (□), and 106.1 °C (⧫). Grey symbols indicate the sample was measured in the power-compensation DSC, with dark grey and light grey symbols representing their black and hollow heat-flux equivalents.

equation had the following form:

$$k^{1/n} = (\beta \times (\text{mass})^{0.5}) + k_0 \tag{5}$$

where k_0 is the theoretical Avrami rate constant of a sample with zero thickness and β is a constant (units of $\text{mass}^{-0.5}$) that describes the effect of the sample size on the observed crystallization rate. Determined values for β and k_0 are listed in Table 3. Negative values of k_0 determined for the LDPE 1.5 sample at certain isothermal crystallization temperatures were a result of data scatter.

Another approach can be used to extrapolate the Avrami growth constant to zero thickness. It has been shown in the literature that $k^{1/n}$ often follows an Arrhenius-type expression [32]:

$$k^{1/n} = A\mathrm{e}^{-E_a/RT_c} \tag{6}$$

$$-\frac{1}{n}\ln(k) = \left(\frac{E_a}{R}\right)\frac{1}{T} - \ln(A) \tag{7}$$

Representative Arrhenius plots are shown in Fig. 13. In the figure, deviation from linearity is noted at the lower crystallization temperatures (higher values of $1/T$) and is more pronounced for thicker samples. These upward deviations are indicative of higher actual sample temperatures; the actual sample temper-

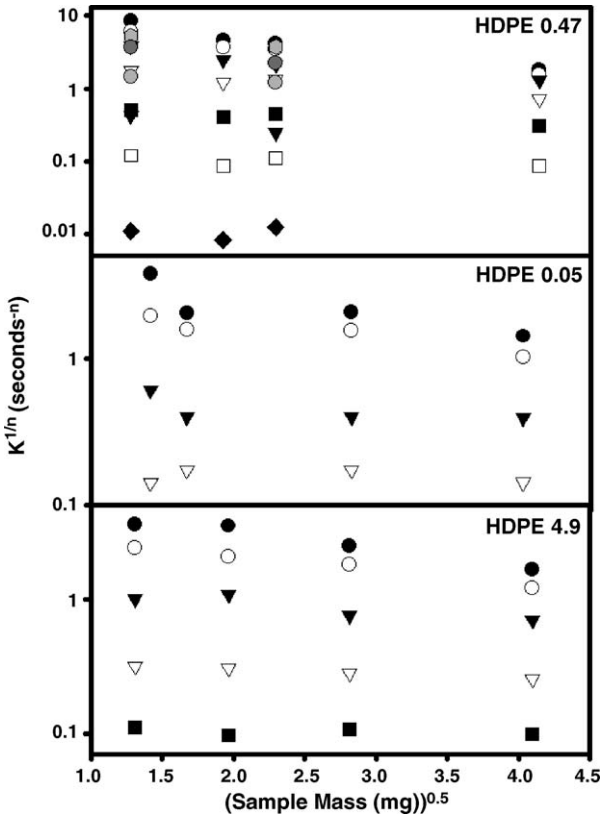

Fig. 11. Plot of $k^{1/n}$ vs. the square root of the sample mass for HDPE samples on a logarithmic scale: 118.5 °C (●), 120.0 °C (◯), 121.4 °C (▼), 122.9 °C (▽), 124.4 °C (■), 125.9 °C (□), and 127.4 °C (♦). Grey symbols indicate the sample was measured in the power-compensation DSC, with dark grey and light grey symbols representing their black and hollow heat-flux equivalents.

atures are roughly the same as what was predicted using the finite difference model. If the samples crystallized at higher crystallization temperatures for longer times are assumed to be void of heat-transfer limitations, a line can be fit through these points and extended to lower temperatures to determine the heat-transfer independent rate constant, i.e. the rate at zero thickness. This extrapolated $k^{1/n}$ is also shown in Table 3. The extrapolated Arrhenius-determined $k^{1/n}$ was much different than the extrapolated value from Eq. (5), in some cases the former was larger in others the former was smaller. We believe the $k^{1/n}$ versus $(\text{mass})^{0.5}$ is more accurate because an Arrhenius relationship is not necessarily a correct description of the behavior.

Transcrystallinity has been presented elsewhere as an explanation of why the rate of crystallization decreases with sample thickness [33,34]. In other words, differences in the relative amounts of transcrystallinity (i.e. nucleation) lead to differences in the crystallization rate as a function of thickness, with thinner samples showing more transcrystallinity and hence higher crystallization rates since the relative amount of sample in contact with the metal pan increases. Certainly, the limiting effect of polymer thermal conductivity has been shown in cases where transcrystallinity cannot be an issue. For example, the melting point of indium will change if a polymer layer is present between indium and the surface [35–37]. Two arguments strongly favor

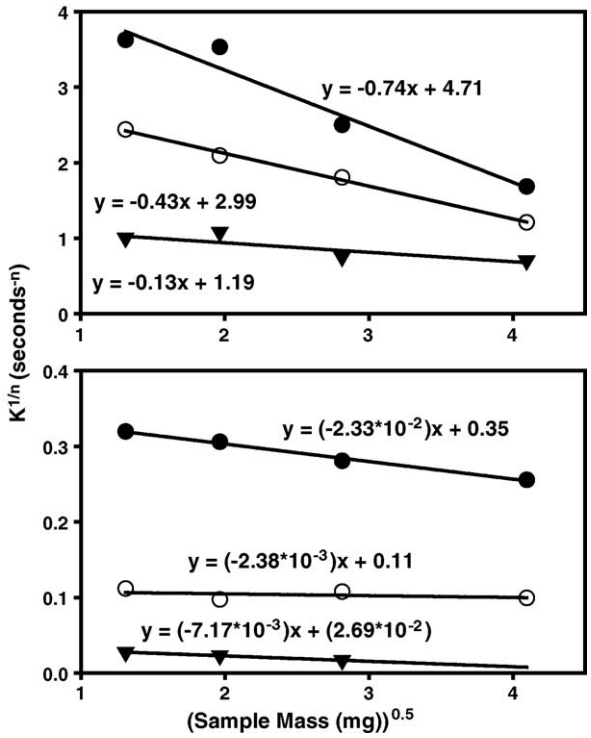

Fig. 12. Linear extrapolation of Avrami parameters to zero thickness (sample is HDPE 0.47) Fig. 13: (a) 118.5 °C (●), 120.0 °C (◯), 121.4 °C (▼) and (b) 123.0 °C (●), 124.4 °C (◯), 125.9 °C (▼).

the thermal conductivity explanation, rather than the transcrystallinity explanation, as causing the rate reduction with sample thickness. The first is that the Avrami exponent shows no consistency with sample thickness; if the differences in the amount

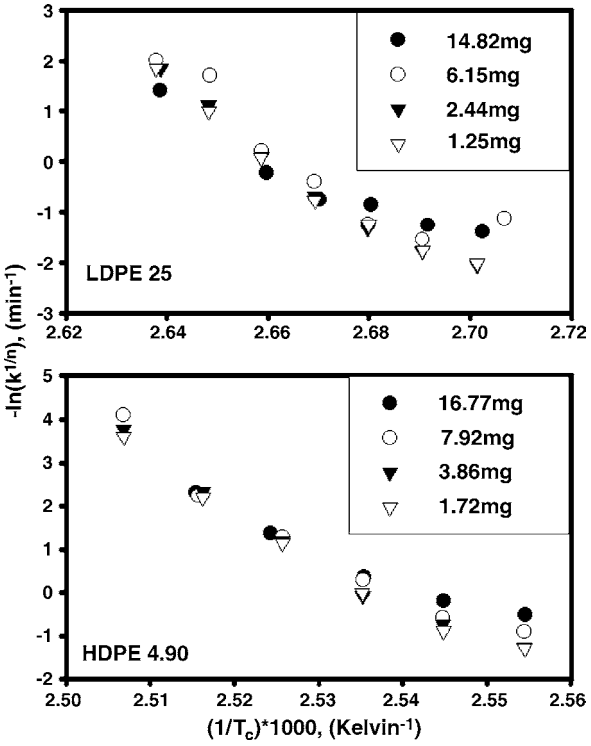

Fig. 13. Arrhenius plots for LDPE 25 and HDPE 4.9 samples.

Table 3
Linear fit parameters to $k^{1/n}$ vs. (sample mass)$^{1/2}$ and k_0 from Arrhenius extrapolation

LDPE	97.1 °C	98.6 °C	100.1 °C	101.6 °C	103.1 °C	104.6 °C	106.1 °C
LDPE 1.5							
k_0	4.18	2.71	1.49	−0.12	0.09	−0.10	−0.02
β	−0.35	0.09	−0.01	0.32	0.08	0.10	0.03
Arrhenius							
k_0	6.84	3.01	1.19	0.54	0.24	0.11	0.05
LDPE 25							
k_0	9.12	7.03	4.28	1.99	0.71	0.53	0.10
β	−1.56	−0.91	−0.45	−0.02	0.12	−0.14	0.03
Arrhenius							
k_0	136.26	54.44	22.59	9.41	3.94	1.63	0.90
LDPE 30							
k_0	5.56	4.10	1.92	0.97	0.40	0.12	0.06
β	−0.80	−0.78	−0.22	−0.11	−0.03	5.7×10^{-3}	1.1×10^{-3}
Arrhenius							
k_0	13.11	4.51	1.83	0.75	0.31	0.13	0.07
HDPE	118.5 °C	120.0 °C	121.4 °C	122.9 °C	124.4 °C	125.9 °C	127.4 °C
HDPE 0.47							
k_0	9.55	6.99	4.33	2.05	0.57	0.12	8.9×10^{-3}
β	−2.00	−1.38	−0.78	−0.33	−0.06	-8.9×10^{-3}	9.0×10^{-4}
Arrhenius							
k_0	775.49	118.80	18.59	2.97	0.48	0.08	0.01
HDPE 0.05							
k_0	3.97	2.23	0.58	0.17	0.04		
β	−0.66	−0.29	−0.05	-3.0×10^{-3}	-3.2×10^{-3}		
Arrhenius							
k_0	32.23	5.43	0.92	0.16	0.03		
HDPE 4.9							
k_0	4.75	2.99	1.22	0.35	0.11	0.04	
β	−0.75	−0.43	−0.13	−0.02	-2.7×10^{-3}	7.1×10^{-3}	
Arrhenius							
k_0	17.42	4.62	1.24	0.32	0.09	0.02	

All tables were determined with the TA Q1000 DSC unless otherwise noted, and all determined values are listed with the following units: k, (min)$^{-n}$;0 n, dimensionless; τ_0, min.

of crystalline material found in an epitaxial structure were significantly different than that in a spherulitic structure, then the Avrami exponents should be different. The second argument is that ratio of the rate of transcrystalline nucleation to the rate of other nucleation steps should not be a function of the temperature, i.e. different thickness samples should have different crystallization rates no matter what the crystallization temperature if the transcrystallinity explanation were correct. In fact, at low temperatures there is a crystallization rate difference between different thicknesses, but at higher temperatures there is no crystallization rate difference, consistent with a thermal conductivity explanation. Note this argument does not mean transcrystallinity is not present; rather our argument is that nucleation is not the rate-limiting step in the fractional crystallinity region of interest.

An issue that remains unaddressed is the actual sample temperature, which would be of importance for using these kinetic parameters in a numerical model. A temperature calibration error clearly exists as demonstrated by the 1.5 °C temperature difference between the two instruments. The correct procedure to accurately determine the sample temperature would have been a −75 °C/min cool followed by an isothermal hold; however, there is no practical way to implement such a calibration. Some liquid crystal transitions can be used to calibrate a DSC upon cooling rather than heating [38]; using a cooling calibration procedure presumably would have yielded a more accurate temperature, although the high rates used in this experiment make this procedure very questionable. Even if the calibration were perfect, a recent paper suggests that the temperature of the crystalline growth face may not be the same as the temperature of the bulk sample due to a temperature gradient across the crystal surface caused partially by the difference in thermal conductivity of the crystalline and amorphous fractions [39]. The extrapolation method presented in this paper would probably not account for this effect since the sample is assumed to be at uniform temperature.

4. Conclusions

Crystallization kinetics were measured for three different LDPE and three different HDPE samples as a function of sample thickness. Sample size does affect the observed rate of crystallization at fast crystallization rates; larger samples tended to crystallize more slowly. The reduction in crystallization rate was attributed to higher sample temperatures caused by the crystallization exotherm. The Avrami rate constant k, which theoretically encompasses all thermal effects, was found to linearly decrease when taken to the inverse power of the Avrami exponent and plotted against the square root of the sample mass. This plot was used to extrapolate zero thickness and determine the true Avrami rate constant k without distortion from thermal conductivity effects. Finally, data and conclusions obtained from a heat-flux DSC were comparable with those from a power-compensation DSC.

Acknowledgements

The authors would like to gratefully acknowledge Dr. Rajendra Krishnaswamy and Barbara Phillips with the Chevron-Phillips Chemical Company for performing measurements with the power-compensation DSC. We also gratefully acknowledge Dr. Joe Domine at Exxon-Mobil Chemical for supplying the HDPEs. Advice from personnel at TA Instruments is also gratefully acknowledged. Mitch would also like to thank his fellow graduate students for their support.

References

[1] Y.K. Godowsky, G.L. Slonimsky, J. Polym. Sci. Polym. Phys. Ed. 12 (1974) 1053.
[2] M.R. Kamal, E. Chu, Polym. Eng. Sci. 23 (1983) 27–31.
[3] T. Ozawa, J. Therm. Anal. Calorim. 64 (2001) 109–126.
[4] G. Höhne, W. Hemminger, H.J. Flammersheim, Differential Scanning Calorimetry, Springer, Heidelberg, 1996.
[5] S.L. Simon, Thermochim. Acta 374 (2001) 55–71.
[6] G.W.H. Höhne, N.B. Shenogina, Thermochim. Acta 310 (1998) 47–51.
[7] S.M. Marcus, R.L. Blaine, Thermochim. Acta 243 (1994) 231–239.
[8] B. Wunderlich, A. Boller, I. Okazaki, K. Ishikiriyama, Thermochim. Acta 304/305 (1997) 125–136.
[9] G.W.H. Höhne, Thermochim. Acta 330 (1999) 45–54.
[10] G.W.H. Höhne, Thermochim. Acta 330 (1999) 93–99.
[11] J.A. Martins, J.J.C. Cruz Pinto, J. Appl. Polym. Sci. 91 (2004) 125–131.
[12] E. Piorkowska, A. Galeski, Polymer 33 (1992) 3985–3989.
[13] E. Piorkowska, J. Appl. Polym. Sci. 66 (1997) 1015–1028.
[14] M. Avrami, J. Chem. Phys. 7 (1939) 1103–1112.
[15] M. Avrami, J. Chem. Phys. 8 (1940) 212–224.
[16] L. Mandelkern, Crystallization of Polymers, McGraw Hill, New York, 1964.
[17] The phrase “where crystallization begins” is, in fact, ill-defined. As is clear, our definition of this critically important parameter is much more pragmatic, and doesn’t really address the underlying polymer physics.
[18] http://www.tainstruments.com/main.asp?n=1&id=89.
[19] P.J. Phillips, Y.H. Kao, Polymer 27 (1986) 1679–1686.
[20] L.E. Alexander, X-Ray Diffraction Methods in Polymer Science, Robert E. Krieger Publishing Company, Malbar, Florida, 1969.
[21] J.D. Menczel, T.M. Leslie, J. Therm. Anal. 40 (1993) 957–970.
[22] J.D. Menczel, J. Therm. Anal. 49 (1997) 193–199.
[23] E2070: Kinetic Parameters by Differential Scanning Calorimetry Using Isothermal Methods, ASTM International, West Conshohocken, PA, (2005).
[24] B.P. Grady, W.B. Genetti, R.J. Lamirand, M. Shah, Polym. Eng. Sci. 41 (2001) 820–829.
[25] H.S. Carslaw, J.C. Jaeger, Conduction of Heat in Solids, Clarendon Press, Oxford, 2004.
[26] G.V. Fraser, A. Keller, J.A. Odell, J. Appl. Polym. Sci. 22 (1987) 2979–2989.
[27] J.D. Hoffman, L.J. Frolen, G.S. Ross, J.I. Lauritzen Jr., J. Res. Natl. Bureau Stand. A Phys. Chem. 79A (1975) 671–699.
[28] Z. Ding, J.S. Spruiell, J. Polym. Sci. Polym. Phys. Ed. 34 (1996) 2783–2804.
[29] Z. Ding, J.S. Spruiell, J. Polym. Sci. Polym. Phys. Ed. 35 (1997) 1077–1093.
[30] P. Supaphol, J.S. Spruiell, J. Polym. Sci. Polym. Phys. Ed. 36 (1998) 681–692.
[31] J.E. Wagner, P.J. Phillips, Polymer 42 (2001) 8999–9013.
[32] P. Cebe, S.D. Hong, Polymer 27 (1986) 1183–1192.
[33] N. Billon, V. Henaff, J.M. Haudin, J. Appl. Polym. Sci. 86 (2002) 734–742.
[34] N. Billon, V. Henaff, E. Pelous, J.M. Haudin, J. Appl. Polym. Sci. 85 (2002) 725–733.
[35] C.P. Camirand, Thermochim. Acta 417 (2004) 1–4.
[36] T. Boddington, P.G. Laye, Thermochim. Acta 115 (1985) 345–350.
[37] G. Hakvoort, L. Van Reijen, A. Aartsen, Thermochim. Acta 93 (1985) 317–320.
[38] S.M. Sarge, G.W.H. Höhne, H.K. Cammenga, W. Eysel, E. Gmelin, Thermochim. Acta 361 (2000) 1–20.
[39] B.X. Gaun, P.J. Phillips, Polymer 46 (2005) 8763–8773.